

Simulations of two-dimensional foam rheology: localization in linear Couette flow and the interaction of settling discs

A. Wyn¹, I.T. Davies¹, and S.J. Cox^{1,2} ^a

¹ Institute of Mathematical and Physical Sciences, Aberystwyth University, Ceredigion SY23 3BZ, Wales, UK

² UMR 5588 – Laboratoire Spectrométrie Physique, B.P. 87, F-38402 St. Martin d’Hères Cedex, France.

January 7, 2008

Abstract. Surface Evolver simulations of flowing two-dimensional foams are described. These are used for two purposes. Firstly, to extract the location of the T_1 s, the changes in bubble topology that occur during plastic flow. It is shown that the T_1 s are localized in space, becoming more so as the polydispersity of the foam decreases. Secondly, the sedimentation of two circular discs through a foam under gravity is studied. If the discs are sufficiently close, they begin to interact and one moves behind the other during their descent.

PACS. 47.57.Bc Foams and Emulsions – 83.80.Iz Emulsions and Foams

1 Introduction

Liquid foams are familiar from domestic use and important in industrial applications including ore-separation and enhanced oil recovery [1, 2]. They are elasto-visco-plastic complex fluids with a highly nonlinear response to applied forces: at low strain they deform elastically, like a solid, while above a yield stress they flow like a viscous liquid [3]. Of all complex fluids, liquid foams provide one of the most experimentally accessible systems for study, since bubbles are objects that can have millimetric dimensions. Moreover, Plateau’s laws [4] mean that the internal structure of a foam is well understood, at least at the level of the network of films. Foams thus provide a prototypical complex fluid.

However, given the degree of disorder within the foam structure and the complex response, it makes sense to first consider two-dimensional (2D) foams, such as can be made by squeezing a foam between parallel glass plates until it consists of a single layer of bubbles [5]. Other realizations of a 2D foam include the bubble raft of Bragg and Nye [6], promoted recently by Dennin and co-workers [7, 8, 9], and the hybrid method of Cyril Stanley Smith [10] and Fortes and co-workers [11, 12]. A theme of current research is exploring the different responses of each of these experimental setups [13, 14], requiring an understanding in particular of the effects of liquid content.

The mathematical idealization of a two-dimensional foam is, however, clear: a dry 2D foam at equilibrium consists of bubbles with fixed areas surrounded

^a email: foams@aber.ac.uk

by films that are circular arcs meeting threefold at angles of 120° (figure 1). These rules are consequences of minimization of energy [15], which is in this case the total film length multiplied by surface tension. This model, and various approximations to it, have long been used for simulation [16, 17, 18, 19, 20, 21]. Here, we use the Surface Evolver software [22] to simulate with high accuracy foams consisting of many hundreds of bubbles, to predict the plastic response of 2D foams.

At low strain a foam responds as an elastic medium. That is, the shear stress, given as a sum of surface tension contributions in the films [23, 24], increases linearly with strain. As the strain increases, the foam begins to yield and bubbles begin to slide past each other in plastic events known as T_1 topological changes (figure 1) [25]. These occur when a film shrinks to zero length and a fourfold vertex is formed. Such a vertex is unstable, and immediately dissociates into two threefold vertices with the connecting film now perpendicular to the vanishing one. In the notation of Wang et al. [9], two bubbles that were nearest-neighbours become next-nearest neighbours, and *vice versa*. Each T_1 event contributes a drop in both total film length and stress.

Localization of T_1 events, also referred to as shear banding, has been described in experiments in an annular wide-gap Couette viscometer [26]. After an initial transient, the majority of T_1 events occur close to the inner moving wall. Similar results have been found in simulations [27]. In linear Couette shear between parallel side-walls, there is also localization of T_1 s. In this geometry, since the shear stress should be homogeneous there is no preferred location for the localized region based upon the boundary conditions, confirmed by Potts model [28] and Surface Evolver [19] simulations.

The presence of phenomena such as shear localization presents a non-trivial obstacle to the development of continuum models for foam rheology [29, 30]. Approaches such as the theory of shear transformation zones [31] also require that the local dynamics is first understood.

In §2 we predict the *width* of the localized region in linear Couette shear, and its dependence on the area disorder of the foam. This is, in effect, a prediction of the degree to which the foam is fluidized under shear. In the limit of zero area disorder - a monodisperse foam - T_1 events tend to occur in a very narrow band and shear-induced crystallization is evident. We show here that making a foam more polydisperse widens the localized region and can thus reduce the amount of static foam present.

We characterize the polydispersity, or volumetric disorder, of a foam by the second moment of the distribution of bubble areas A :

$$\mu_2(A) = \left\langle \frac{(A - \langle A \rangle)^2}{\langle A \rangle^2} \right\rangle \quad (1)$$

where $\langle \rangle$ denotes an average over the whole foam. In contrast to the disorder in the number of sides n of each bubble, $\mu_2(n) = \langle (n - 6)^2 \rangle$, which varies in time due to T_1 s, the area disorder is fixed in each of our simulations. That is, we exclude inter-bubble gas diffusion (coarsening) and film collapse. The elastic response of a foam is characterized by the shear modulus [32], which decreases by up to 10% at both high topological and high volumetric disorder [23].

In a further effort to understand the response of a foam, we consider a geometry in which we know approximately where the T_1 s will occur, and ask what is the interaction between the foam flow and an embedded object (§3).

A number of authors have studied the flow of a 2D foam past a fixed object, with both experiments [12, 33, 34, 35] and simulations [36, 35]. The drag and lift forces on the object are due to a number of contributions. At low velocity the dominant ones are the force from the tensions in the films attached to the object and the pressures in the bubbles that touch it. For a circular object in the centre of a channel the drag force increases with object diameter [36, 37] and decreases with increasing liquid fraction [35]. For asymmetric objects such as an aerofoils [12], and for circular objects

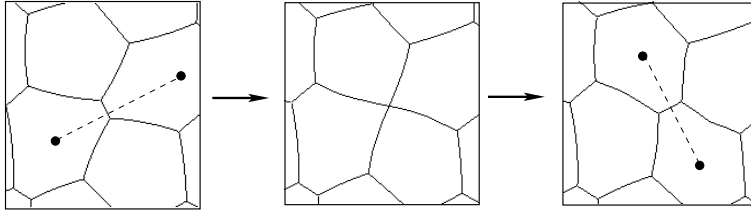


Fig. 1. An ideal 2D foam consists of films that are circular arcs, meeting at 120° . The sequence of images shows a T_1 topological change. The intermediate step with the fourfold vertex is energetically unstable. The orientation of a T_1 is characterized by the lines joining bubble centres adjacent to the deleted and created films, marked by dashed lines.

close to one of the walls of the channel, there is in addition a lift force. For an aerofoil this is a negative lift [12], while for the circular object it points away from the wall [36].

Related work in three dimensions is concerned with single spheres, with a diameter larger than the bubble size, being pulled [38, 39, 40] or dropped [41, 42] through a foam.

In §3 we examine the interaction between two circular discs falling through a foam under their own weight. We aim to answer questions such as the conditions under which two objects falling through a foam are mutually attracted or repelled, as has been done for a number of viscoelastic fluids [43, 44, 45]. The answers will give guidance in determining the effect of a wake in a discretized elasto-plastic fluid.

To guide our intuition we recall work on the flow of a foam past an ellipse: Doleet et al. [46] found that the only stable orientation of an ellipse was with its long axis parallel to the direction of flow. This is a feature of elastic fluids [47]. Is it therefore the case that the plastic events are not significant in determining this aspect of the foam response, and we can treat it as an elastic liquid?

2 The localization of topological changes in linear Couette shear

We describe simulations of the slow linear Couette shear of a 2D foam confined between parallel walls (figure 2). The area

dispersity $\mu_2(A)$ is varied to determine how the width of the localized region depends upon this parameter.

2.1 Method

We use the Surface Evolver [22] in a mode in which each film is represented as a circular arc. We use foams of $N = 1120$ bubbles, in a channel of width $W = 3.2$ and length $L = 8.0$, giving an average bubble size of $\langle A \rangle = 0.0229$ and about 21 bubbles between the walls. The value of surface tension, which should be thought of as a line tension with units of energy per unit length, is taken equal to one throughout. A realistic foam structure is found by minimizing the total film length subject to the prescribed bubble areas. For some parameter values we doubled the number of bubbles in the x -direction to ensure that the results were not affected by the possibility of system-wide avalanches of T_1 events (data not shown).

The simulation procedure is as follows. A Voronoi construction [48] is first used to generate a fully periodic tessellation of the plane. Bubbles at the top and bottom are sequentially deleted until the required number of bubbles remains. This structure is imported into the Surface Evolver and peripheral films constrained to one of the two side-walls, a distance W apart. New bubble areas are determined randomly from a Weibull distribution:

$$f(A; \beta, \lambda) = \frac{\beta}{\lambda} \left(\frac{A}{\lambda} \right)^{\beta-1} e^{-(A/\lambda)^\beta}. \quad (2)$$

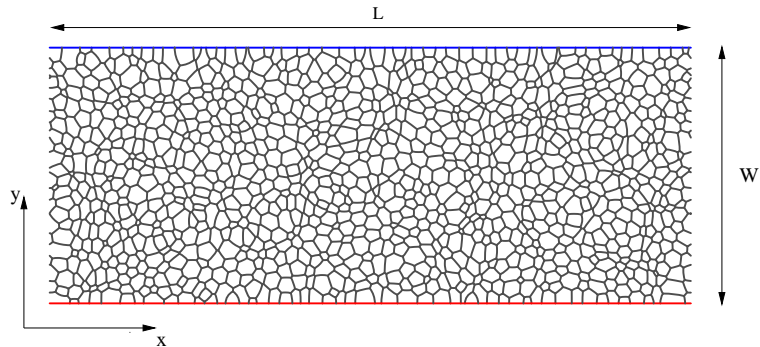


Fig. 2. An example of the foams used to simulate linear Couette shear in a channel, with $\mu_2(A) = 0.175$. The channel is periodic in the x direction. To shear the foam the side-wall at the top of the image is moved to the right (positive x -direction) in small increments $d\epsilon$. Those films that meet the side-walls have their ends pinned to the wall (no-slip condition).

The parameter $\beta > 1$ determines the area dispersity and the parameter λ is chosen as $\lambda = 1.115\langle A \rangle$ (so that the peak of the distribution is close to $A = \langle A \rangle$). The second moment of this distribution is

$$\mu_2(A) = \frac{\Gamma\left(1 + \frac{2}{\beta}\right)}{\Gamma\left(1 + \frac{1}{\beta}\right)^2} - 1 \quad (3)$$

where Γ is the Gamma function. The limit $\beta \rightarrow \infty$ corresponds to a monodisperse foam ($\mu_2(A) = 0$); decreasing β leads to increasingly polydisperse foams. Note that since our foam sample is finite, the value of β chosen for each simulation can lead to slightly different values of $\mu_2(A)$.

The initial structure for each simulation is found by reducing the total film length to a local minimum. During this minimization T_1 s are triggered by deleting each film that shrinks below a certain length l_c and allowing a new films to form to complete the process. The critical length l_c is a measure of liquid fraction ϕ [36], but we keep it small enough here ($l_c = 0.005$ throughout, corresponding to $\phi = 2.6 \times 10^{-4}$) that it should not affect the results [27].

To shear the foam, a small step in strain is applied by moving one of the confining walls a distance $d\epsilon$, moving all vertices affinely, and then reducing the film length to a minimum. In this way,

the foam passes through a sequence of equilibrium states, appropriate to an applied strain with strain rate much lower than the rate of equilibration after T_1 s. The value $d\epsilon = 0.0078$ was used throughout, and the foam sheared up to a total strain of at least $\epsilon = 5$.

2.2 Position of T_1 s

Figure 3 shows the T_1 positions in foams at three representative values of $\mu_2(A)$. Plotting the y position of a T_1 against strain, or the number of iterations, indicates that for each value of $\mu_2(A)$ there is an initial transient that lasts up to approximately unit strain. In the monodisperse case shown in figure 3(a), the T_1 s mostly occur close to the moving wall. Although this is not the case for all of our simulations in the monodisperse limit, we found that monodisperse foams usually localize near one of the walls (see figure 4(a)). As the polydispersity increases, the width of the localized region increases and it often occurs further from the walls (figure 4(a)). At large values of polydispersity (small β) the T_1 s occur almost throughout the channel. For the intermediate value of $\mu_2(A)$ shown in figure 3(b), we note that plotting the data on y vs x axes illustrates a slight undulation in the localized region.

We measure the width l_w of the localized region as follows. After the tran-

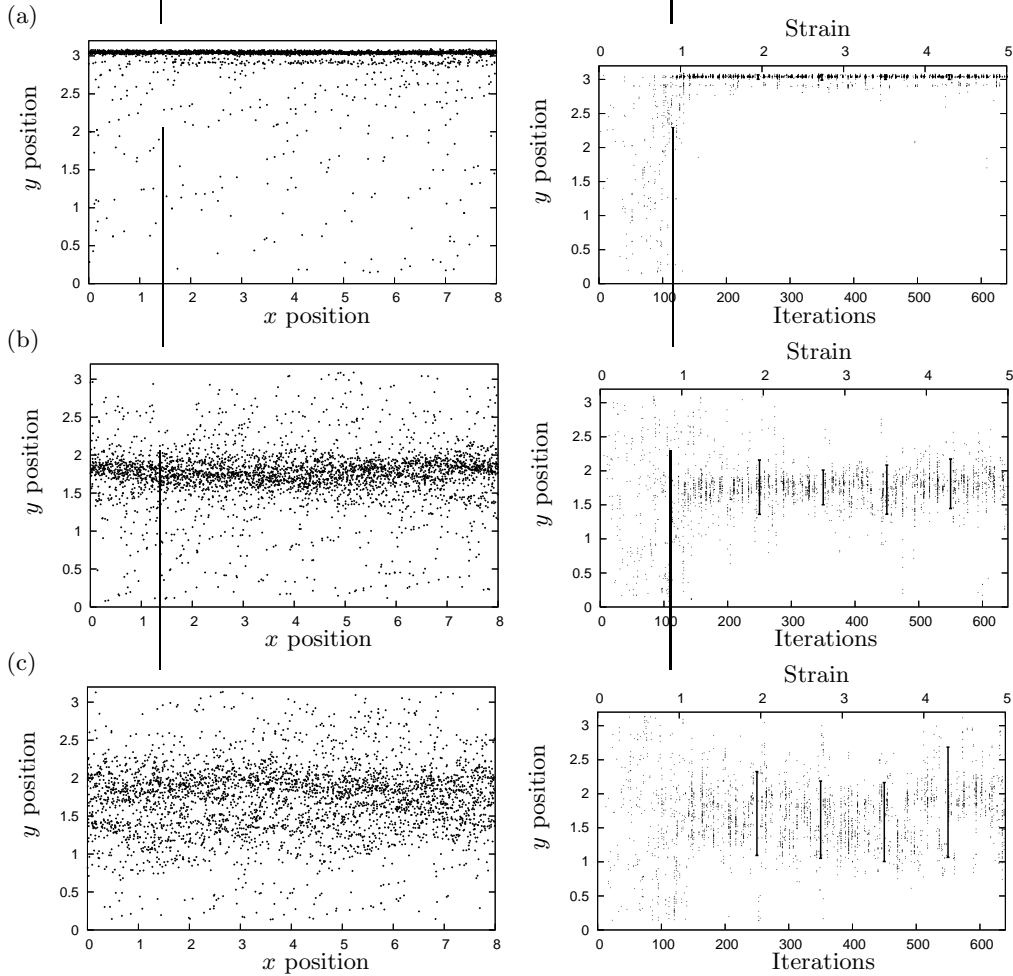


Fig. 3. Locations of topological changes in simulations at three values of $\mu_2(A)$, shown on y vs x axes (left-hand column) and on y vs γ (strain or number of iterations) axes (right hand column). (a) Monodisperse ($\mu_2(A) = 0, \beta \rightarrow \infty$). (b) Moderately polydisperse (the foam in figure 2, $\mu_2(A) = 0.175$). (c) Highly polydisperse ($\mu_2(A) = 0.561$). The vertical bars show the position and width of the localized region after the transient; they are centred at the average y position of the T_1 s, averaged in groups of $N_s = 100$ iterations, and their total height encompasses the foam width within which 90% of T_1 s occur.

sient, taken to be the first 200 iterations, we find the mean y position of the T_1 s in bins of N_s iterations. The localisation width w_l is the interval in y position within which 90% of T_1 s are found. We find that $N_s = 100$ gives the best measure of w_l , that is, it balances the need to have many points in each bin with the desire to accurately reflect the width of the evolving localization.

Figure 4(b) shows the increase of localisation width w_l/W with disorder. It

is clear that at high disorder, and for narrow (low W foams), the localized region may encompass the whole foam. At low disorder, crystallization is more frequent, and localization usually occurs in a narrow band. We find the following rule of thumb:

$$\frac{w_l}{W} \approx \sqrt{\mu_2(A)}. \quad (4)$$

On a few occasions (data not shown) we found that two narrow localized regions persisted up to strains of about 3.

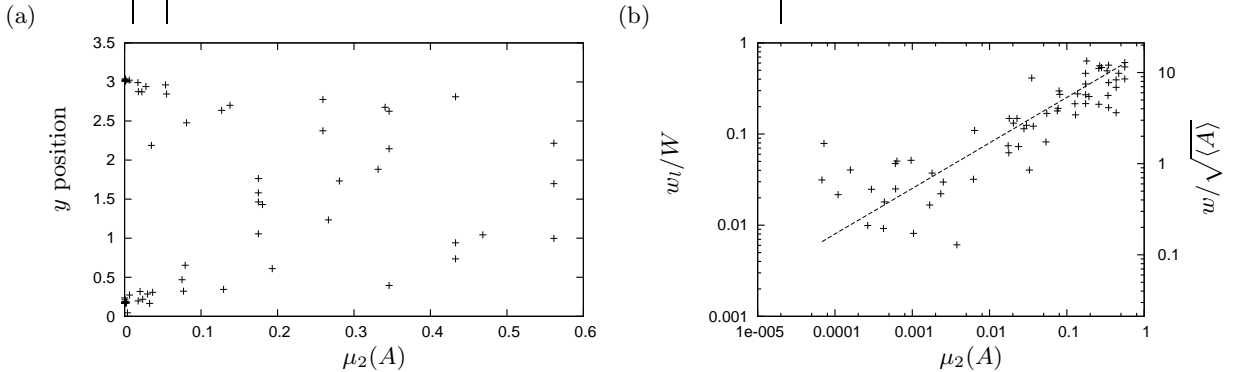


Fig. 4. (a) The position of the centre of the localized region, given as the average of the mean y position of the T_1 s in each group of $N_s = 100$ iterations after the transient. Each point corresponds to one full simulation. As the foam becomes less disordered, the T_1 s localize closer to the walls, but without showing a preference for either the stationary or moving wall. (b) The width of the localized region w_l/W , given as the width of foam within which 90% of T_1 s occur after the transient, increases with area disorder $\mu_2(A)$. Note the log axes. The right-hand axis indicates the localization width in terms of bubble diameters. The straight line has slope one-half: $w_l/W = 0.8\sqrt{\mu_2(A)}$.

2.3 Angular dependence of T_1 s

Wang et al. [9] recorded the orientation of the disappearing film and the newly-created film during each T_1 event in their experiments on a sheared bubble raft. This is done by drawing a line between the centres of the bubbles neighbouring each film, in consecutive images bracketing the T_1 event, as in figure 1. The distributions of angles show peaks at angles of about 45° and 135° respectively to the walls of the channel. The height of the peak increases with shear-rate, and at low shear rate a small “knee” appears at about 90° , i.e. parallel to the direction of shear.

From our simulations we can extract the same data, in the limit of low shear-rate. Figure 5 shows these distributions, with data obtained after the transient in each simulation. We find the same peak for the films that disappear, but the most probable orientation for new films is at 30° . Moreover, no detail is seen around 90° . We therefore believe that this discrepancy is due to the high liquid content in the bubble raft experiments, unattainable with the methods described here.

Although we do not probe the effect of shear-rate on the height of the peak

(as could be done with the Viscous Froth Model [49]), we see that it is strongly affected by polydispersity: monodisperse foams exhibit a much higher peak. This is perhaps suggestive of hexagonal ordering, although we did not test this explicitly (e.g. by measuring $\mu_2(n)$, with n the number of sides of a bubble).

2.4 Other predictions

Our ultimate goal is to predict the region of a foam where localization will occur from the initial structure. Given that there are many T_1 s throughout the foam during the transient, this is difficult. To begin, we seek ways of characterizing the foam structure, and then following these characterizations through each simulation to detect robust changes when the foam localizes. In particular, these methods should be able extractable from a single image of a foam at a given time, rather than requiring the tracking of bubbles from video analysis.

Our structural measures extract the distribution of various quantities as a function of y . In particular, we seek to characterize the area distribution of a foam. Five methods were investigated:

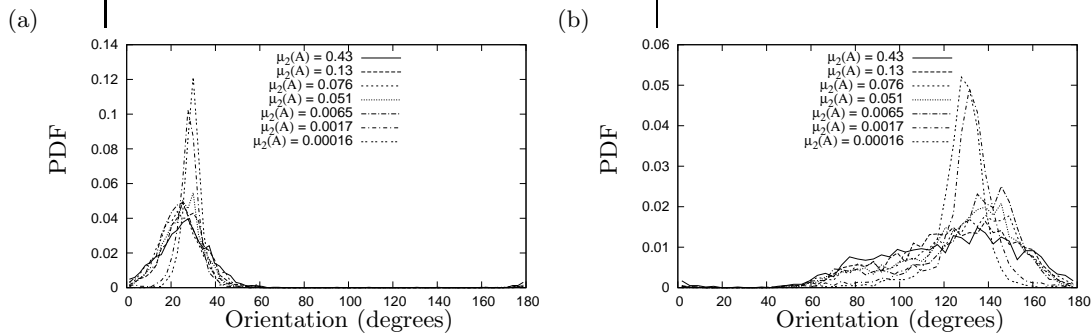


Fig. 5. The distribution of the angle made with the x axis by a line joining the centres of the two bubbles neighbouring a film that (a) disappears and (b) is created during a T_1 event. The former peaks at around 30° and the latter at 135° .

1. we find the centre (x_c, y_c) of each bubble by averaging the coordinates of its vertices, and calculate the histogram of y_c in 20 bins;
2. for each value of $y_0 \in [0, W]$ we calculate the average area \mathcal{A}_y of those bubbles that intersect the line $y = y_0$;
3. we find the centre (x_c, y_c) of each bubble by averaging the coordinates of its vertices, and calculate the local foam disorder $\mu_2(A)$, from (1), in 20 bins based upon y_c ;
4. for each value of $y_0 \in [0, W]$ we calculate the average length \mathcal{L}_y of the line $y = y_0$ that is covered by each bubble, sometimes referred to as the linear intercept method [50];
5. we calculate the texture tensor [51] based upon bubble centres in 20 bins.

Figure 6 shows these structural measures for the foam in figures 2 and 3(b) at the beginning and end of the simulation, i.e. before and after localization has occurred. All measures are uniform at the beginning of the simulation, suggesting that it is not possible to predict where a foam will localize.

Method 4, \mathcal{L}_y , is the only 1D structural measure to give a clear indication that the foam has localized. Note that it does have the disadvantage that large fluctuations are observed for ordered structures.

The texture tensor, method 5, is the tensorial equivalent of \mathcal{L}_y . It is more sensitive than the latter but more difficult to extract from the data. We shall return

to it in future work, in addition to other measures such as the local stress in the foam.

3 Movement of discs through a foam

We describe simulations that probe the interaction between macroscopic objects falling through a foam. The system under study consists of two circular discs, whose diameters are equal and larger than the bubble size. Recall that an elliptical object tries to align itself with the foam flow [46]. Here, we show that when the discs are sufficiently close, one of them moves behind the other.

The discs' motion is commenced from a position near the top of a monodisperse foam. They descend under the action of three forces, defined in figure 7: (i) gravity; (ii) the resultant tension force F^n due to the network of films that contact each obstacle; (iii) the resultant pressure force F^p from the bubbles that touch each obstacle. The films touching the discs are not uniformly distributed around the circumference: as figure 8(a) shows, they bunch up behind the obstacle. It is this inhomogeneity that leads to the resultant network and pressure forces.

For each disc the network force is a sum over those films j that touch the disc. Each film meets the disc perpendicularly, and makes an angle θ with the

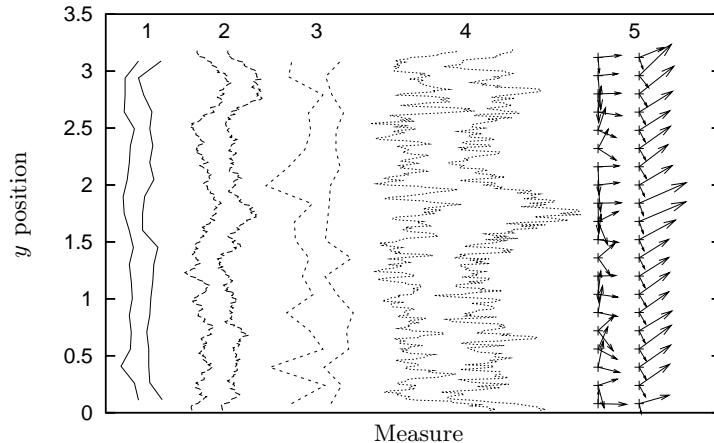


Fig. 6. The five measures of foam structure are shown from left to right for the foam in figure 3(b), both at the beginning and the end of the simulation. It is clear that the foam is initially fairly isotropic, and that none of the methods 1 to 3 indicate that any structural change has occurred during the evolution. In contrast, the peak around $y \approx 1.7$ in \mathcal{L}_y (method 4) corresponds to the region where the T_1 s have localized. The tensorial texture tensor (method 5) also shows this feature, as well as indicating that the bubbles are more closely aligned (cf. figure 5).

y direction [36]. Thus:

$$\underline{F}^n = \gamma \sum_{\text{films } j} (\sin \theta_j, \cos \theta_j). \quad (5)$$

The pressure force is a sum over all bubbles touching the obstacle:

$$\underline{F}^p = \sum_{\text{bubbles } k} p_k l_k (\sin \theta_k, \cos \theta_k). \quad (6)$$

where p_k is the pressure inside the bubble, l_k is the length of contact, and θ_k is the angle that the inward normal at the midpoint of the line of contact makes with the y -direction.

3.1 Method

We perform quasi-static simulations as described in §2.1, using a foam with $N = 727$ bubbles, width $W = 0.792$ and length $L = 1$. The bubble size is therefore $A \approx 1 \times 10^{-3}$ (it shrinks slightly in proportional to the disc size, since the total area of the foam and two disc system is constant). The cut-off length for T_1 events is $l_c = 0.002$, corresponding to a dry foam with $\phi \approx 1 \times 10^{-3}$. The channel

is periodic in the y direction, parallel to the direction of gravity, and we stop the simulations before either of the discs returns to the top of the foam. Films that meet the side-walls have that end fixed throughout each simulation (no-slip condition). The ends of films that touch the discs are free to slide, so as to be able to make an equilibrium 90° angle (slip condition).

Our dimensionless units are chosen so that the line tension γ has the value 1. We choose the discs to have equal areas in the range $2A$ to $7A$ and equal weights of $w = 10$ irrespective of their size. We first ensured that this value of weight is large enough that the discs are not brought to a halt by the opposing forces due to film tensions and bubble pressures.

Two starting configurations are chosen, as shown in figure 8. The disc centres are initially separated by a distance d_i , either horizontally ($i = 1$) or vertically ($i = 2$). In the first configuration, there is a possibility of a small lift force due to, and perpendicular to, the walls [36], acting to push the discs together; we quantify this in §3.2 and show that

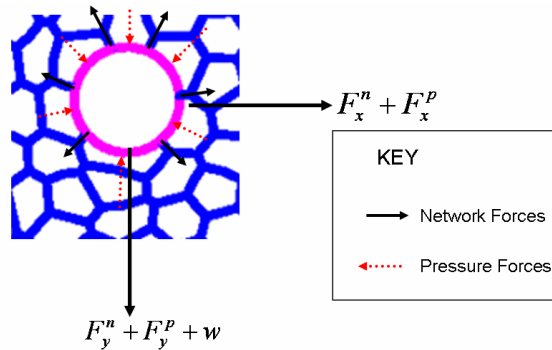


Fig. 7. The position of each disc evolves under the gravitational, tension and pressure forces shown.

the discs are far enough from the wall that it is negligible. The second case has the advantage that the lift force on each disc should be zero on average.

The simulations proceed as follows. A foam containing the two discs in their starting positions is relaxed to equilibrium, using the method described in [35]. At each iteration, the resultant forces on each disc in the x and y directions are calculated and the disc centres moved according to

$$\begin{aligned} \Delta x &= \epsilon (F_x^n + F_x^p), \\ \Delta y &= \epsilon (F_y^n + F_y^p + w), \end{aligned} \quad (7)$$

where the subscripts denote the x and y components of the forces. The parameter $\epsilon = 5 \times 10^{-4}$ measures how far the centres are moved at each iteration. The foam perimeter (energy) is then brought back to a local minimum with the discs fixed. This comprises one iteration, which is repeated until a disc reaches the bottom of the simulation cell. Representative paths of two discs are shown in figure 9.

3.2 Wall effects

To estimate the effect to which the lateral movement observed is due to the wall, we ran simulations for each configuration with and without one of the discs present. For a simulation of configuration 1 in which the discs are far enough apart that they do not interact,

in contrast to figure 9(a), figure 10(a) shows that the motion of the left-hand disc changes little when the right-hand disc is removed. We therefore surmise that the wall has no influence on the motion of the discs here.

In configuration 2, figure 10(b) shows that the lower disc perturbs the foam in such a way that the upper disc moves more quickly than if it were not present. Neither disc moves sideways to a great extent.

3.3 Varying disc size

We now fix the initial centre-to-centre separation of the discs and measure how the separation evolves during the descent for discs of different size. For configuration 1, figure 11 shows that, in general, the area of the discs makes little difference. In all but one case one of the discs falls behind the other one. That our system always chooses the left-hand disc is probably an artefact due to the foam creation step.

Fixing the initial centre-to-centre separation of the discs in configuration 2 leads to the result, shown in figure 12, that the distance between the discs is reduced more quickly when the discs are smaller. This can be attributed to the fact that smaller discs experience a smaller drag force [36], and are therefore more affected by small changes in the foam structure in the wake of another disc.

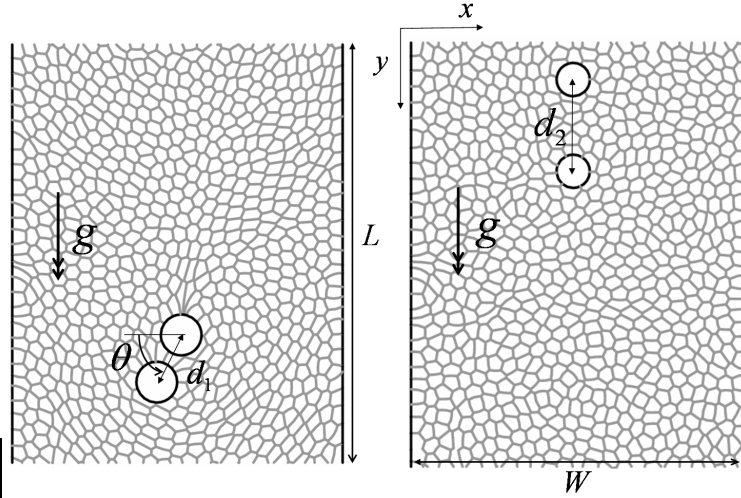


Fig. 8. Two discs in a monodisperse 2D foam confined in a channel of width W . (a) Configuration 1, in which the discs start side-by-side, with a distance d_1 between their centres and an angle θ made by the line joining their centres. (b) Configuration 2, in which the discs start one above the other a distance d_2 apart.

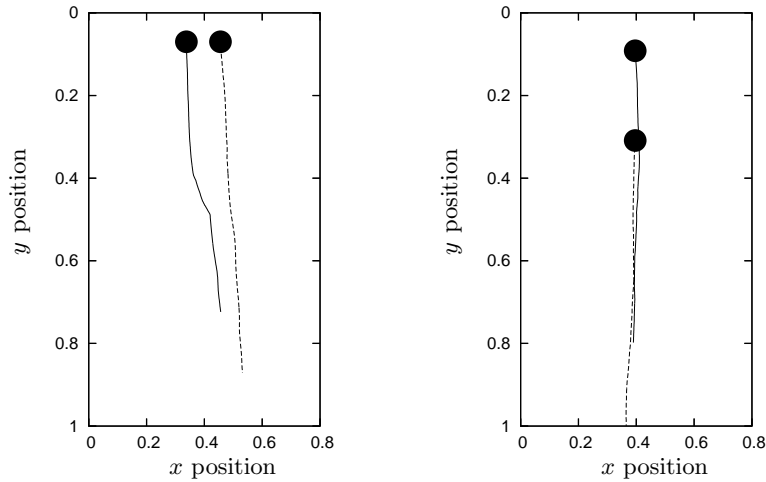


Fig. 9. The motion of the disc centres in two typical simulations. Disc area is $4.5A$. (a) Configuration 1, with $d_1 = 0.08$. Here, both discs move a small distance to the right, and the disc that began on the left of the foam advances more slowly and moves behind the right-hand disc. (b) Configuration 2, with $d_2 = 0.2$. The discs barely deviate to the sides, but the higher disc moves slightly faster in the wake of the lower one.

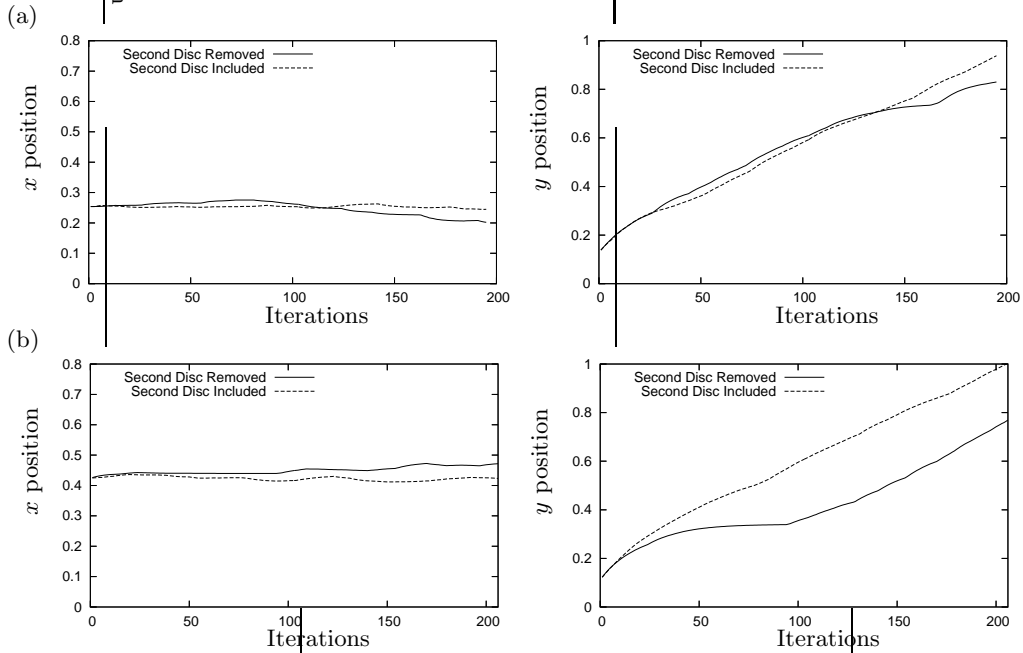


Fig. 10. The position of the disc centres with disc area $3.5A$. (a) In configuration 1, the presence of the right-hand disc (with $d_1 = 0.24$) does not affect the descent of the left-hand one. (b) In configuration 2, the upper disc descends more quickly when the lower disc (a distance $d_2 = 0.2$ away) is present, but they do not deviate sideways.

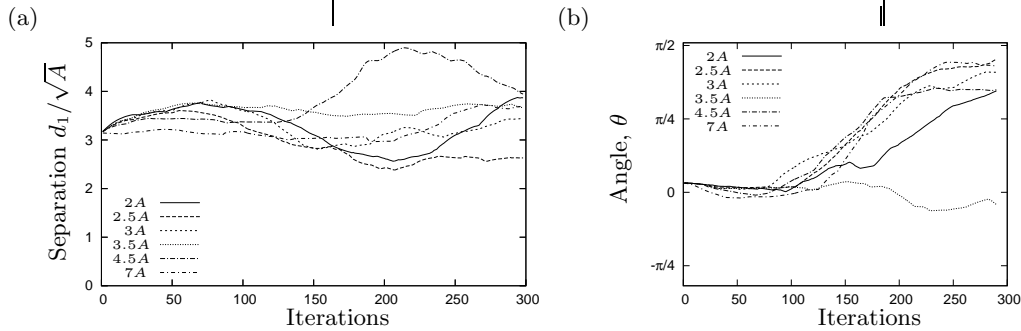


Fig. 11. (a) The separation, measured in bubble widths, of the disc centres in configuration 1 for a range of disc areas, expressed in multiples of the bubble area. The initial separation is close to 3 bubble widths. On average there is a slight increase in the separation between the discs, and no clear trend with disc size. (b) The angle θ made by the line joining the disc centres. In all but one case the left-hand disc moves behind the right-hand one.

3.4 Varying disc separation

The results for configuration 1 in figure 11 may be difficult to interpret because the distance between the edges of the discs varies as well as their areas. This means that there are a different number of bubbles between the discs in each case. We now fix the disc size and vary the ini-

tial separation between the edges of the discs. Figure 13 emphasizes that discs which start closer together are more likely to interact, and for one to move behind the other.

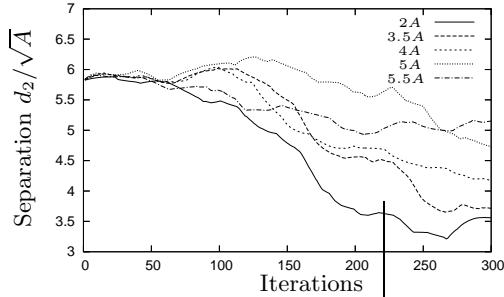


Fig. 12. The separation, measured in bubble widths, of the two discs in configuration 2. The upper disc “catches up” the lower disc, and it does so more quickly if the discs are smaller.

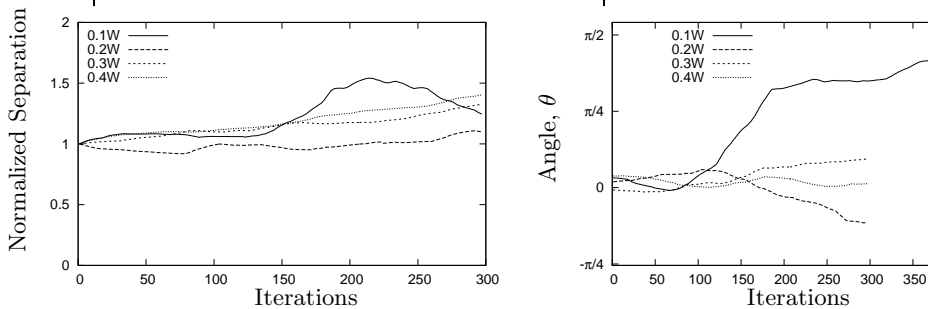


Fig. 13. The separation, normalized by the initial separation, and the angle made by the line joining the centres of the two discs in Configuration 1. The initial separations in the key are given in terms of the width W of the foam. For the closest discs, the left-hand disc moves behind the right-hand one, while for the next closest pair the reverse occurs.

4 Conclusion

We have shown that localization in the linear Couette shear of a 2D foam is highly dependent on the polydispersity in bubble areas. At high dispersity, the localized region can extend throughout the foam, with the width of this region dependent upon the square-root of the second moment of area disorder, $\mu_2(A)$. A signature of the localization is given by a 1D measure of the polydispersity, \mathcal{L}_y , enabling us to probe how bubbles readjust to the shear and allow T_{1s} to collect in specific regions of the foam.

The results begin to explain why the simulations of Kabla and Debrégeas [52] indicate that T_{1s} occur close to the walls: the area dispersity is low in their case, so that we expect the localised region to be near a wall.

Our simulations of two discs descending through a foam probe the interac-

tions between falling objects. We have shown that small particles move faster in the wake of another, and that for sufficiently close pairs of particles one is attracted into the wake of the other. Given the elastic nature of the interaction, and the discrete nature of the foam which allows single bubbles to detach from the disc and possibly move upwards, we are currently working towards extracting the bubble displacement field to test for the phenomenon of a “negative wake” [53].

It remains to investigate the effects of a polydisperse foam, although we expect these to be small, and the interaction between more particles/discs. We are currently pursuing an experimental realization of this system, to ascertain the applicability of the results given here.

For both systems studied here, and indeed for foam research in general, the influence of liquid is important. Extending this work to wet foams presents a

challenge to simulation, although this is itself overshadowed by the demands of three-dimensional calculations on wet foams.

Acknowledgements

We thank K. Brakke for developing, distributing and supporting the Surface Evolver and for providing the script to generate Voronoi input. This work benefited from discussions with D. Weaire, K. Krishan and F. Graner. Financial support is gratefully acknowledged from EPSRC (EP/D048397/1, EP/D071127/1) and the British Council Alliance programme.

References

1. J.J. Bikerman. *Foams: Theory and Industrial Applications*. Reinhold, New York, 1953.
2. R.K. Prud'homme and S.A. Khan, editors. *Foams: Theory, Measurements and Applications*, volume 57 of *Surfactant Science Series*. Marcel Dekker, New York, 1996.
3. D. Weaire and S. Hutzler. *The Physics of Foams*. Clarendon Press, Oxford, 1999.
4. J.A.F. Plateau. *Statique Expérimentale et Théorique des Liquides Soumis aux Seules Forces Moléculaires*. Gauthier-Villars, Paris, 1873.
5. C.S. Smith. The Shape of Things. *Scientific American*, 190:58–64, 1954.
6. L. Bragg and J.F. Nye. A dynamical model of a crystal structure. *Proc. R. Soc. Lond.*, A190:474–481, 1947.
7. J. Lauridsen, M. Twardos, and M. Dennin. Shear-induced stress relaxation in a two-dimensional wet foam. *Phys. Rev. Lett.*, 89:098303, 2002.
8. M. Twardos and M. Dennin. Comparison between step strains and slow steady shear in a bubble raft. *Phys. Rev. E*, 71:061401, 2005.
9. Y. Wang, K. Krishan, and M. Dennin. Statistics of microscopic yielding in sheared aqueous foams. *Phil. Mag. Letts.*, 87:125–133, 2007.
10. C.S. Smith. Grain shapes and other metallurgical applications of topology. In *Metal Interfaces*, pages 65–108. American Society for Metals, Cleveland, OH, 1952.
11. M.E. Rosa and M.A. Fortes. Development of bamboo structure in a 2D liquid foam. *Europhys. Lett.*, 41:577–582, 1998.
12. B. Dollet, M. Aubouy, and F. Graner. Inverse Lift: a signature of the elasticity of complex fluids. *Phys. Rev. Lett.*, 95:168303, 2005.
13. M.F. Vaz and S.J. Cox. Two-bubble instabilities in quasi-two-dimensional foams. *Phil. Mag. Letts.*, 85:415–425, 2005.
14. Y. Wang, K. Krishan, and M. Dennin. Impact of boundaries on velocity profiles in bubble rafts. *Phys. Rev. E*, 73:031401, 2006.
15. J.E. Taylor. The structure of singularities in soap-bubble-like and soap-film-like minimal surfaces. *Ann. Math.*, 103:489–539, 1976.
16. D. Weaire and J.P. Kermode. Computer simulation of a two-dimensional soap froth I. Method and motivation. *Phil. Mag. B*, 48:245–249, 1983.
17. F. Bolton and D. Weaire. The effects of Plateau borders in the two-dimensional soap froth. II. General simulation and analysis of rigidity loss transition. *Phil. Mag. B*, 65:473–487, 1992.
18. T. Okuzono, K. Kawasaki, and T. Nagai. Rheology of Random Foams. *J. Rheol.*, 37:571–586, 1993.
19. S.J. Cox, D. Weaire, and J.A. Glazier. The rheology of two-dimensional foams. *Rheol. Acta*, 43:442–448, 2004.
20. I. Cantat and R. Delannay. Dynamical transition induced by large bubbles in two-dimensional foam flows. *Phys. Rev. E*, 67:031501, 2003.
21. S.J. Cox. The mixing of bubbles in two-dimensional foams under exten-

- sional shear. *J. Non-Newtonian Fl. Mech.*, **137**:39–45, 2006.
22. K. Brakke. The Surface Evolver. *Exp. Math.*, **1**:141–165, 1992.
 23. S.J. Cox and E.L. Whittick. Shear modulus of two-dimensional foams: The effect of area dispersity and disorder. *Eur. Phys. J. E*, **21**:49–56, 2006.
 24. A.M. Kraynik, D.A. Reinelt, and F. van Swol. The structure of random monodisperse foam. *Phys. Rev. E*, **67**:031403, 2003.
 25. D. Weaire and N. Rivier. Soap, cells and statistics—random patterns in two dimensions. *Contemp. Phys.*, **25**:59–99, 1984.
 26. G. Debrégeas, H. Tabuteau, and J.M. di Meglio. Deformation and flow of a two-dimensional foam under continuous shear. *Phys. Rev. Lett.*, **87**:178305, 2001.
 27. S.J. Cox. Simulations of Two-Dimensional Foam under Couette Shear (preprint), 2007. <http://hdl.handle.net/2160/323>.
 28. Y. Jiang, P.J. Swart, A. Saxena, M. Asipauskas, and J.A. Glazier. Hysteresis and Avalanches in two-dimensional foam rheology simulations. *Phys. Rev. E*, **59**:5819–5832, 1999.
 29. E. Janiaud, D. Weaire, and S. Hutzler. Two dimensional foam rheology with viscous drag. *Phys. Rev. Lett.*, **97**:038302, 2006.
 30. P. Marmottant and F. Graner. An elastic, plastic, viscous model for slow shear of a liquid foam. *Euro. Phys. J. E*, **23**:337–347, 2007.
 31. M.L. Falk and J.S. Langer. Dynamics of viscoplastic deformation in amorphous solids. *Phys. Rev. E*, **57**:7192–7205, 1998.
 32. N.P. Kruyt. On the shear modulus of two-dimensional liquid foams: a theoretical study of the effect of geometrical disorder. *J. Appl. Mech.*, **74**:560–567, 2007.
 33. B. Dollet, F. Elias, C. Quilliet, C. Raufaste, M. Aubouy, and F. Graner. Two-dimensional flow of foam around an obstacle: Force measurements. *Phys. Rev. E*, **71**:031403, 2005.
 34. B. Dollet and F. Graner. Two-dimensional flow of foam around a circular obstacle: local measurements of elasticity, plasticity and flow. *J. Fl. Mech.*, **585**:181–211, 2006.
 35. C. Raufaste, B. Dollet, S. Cox, Y. Jiang, and F. Graner. Yield drag in a two-dimensional foam flow around a circular obstacle: Effect of liquid fraction. *Euro. Phys. J. E*, **23**:217–228, 2007.
 36. S.J. Cox, B. Dollet, and F. Graner. Foam flow around an obstacle: simulations of obstacle-wall interaction. *Rheol. Acta.*, **45**:403–410, 2006.
 37. B. Dollet, F. Elias, C. Quilliet, A. Huillier, M. Aubouy, and F. Graner. Two-dimensional flows of foam: drag exerted on circular obstacles and dissipation. *Coll. Surf. A*, **263**:101–110, 2005.
 38. J.R. de Bruyn. Transient and steady-state drag in foam. *Rheol. Acta*, **44**:150–159, 2004.
 39. I. Cantat and O. Pitois. Mechanical probing of liquid foam ageing. *J. Phys.: Condens. Matter*, **17**:S3455–S3461, 2005.
 40. I. Cantat and O. Pitois. Stokes experiment in a liquid foam. *Phys. Fluids*, **18**:083302, 2006.
 41. S.J. Cox, M.D. Alonso, S. Hutzler, and D. Weaire. The stokes experiment in a foam. In P. Zitha, J. Banhart and G. Verbist, editor, *Foams, emulsions and their applications*, pages 282–289. MIT-Verlag, Bremen, 2000.
 42. H. Tabuteau, F.K. Oppong, J.R. de Bruyn, and P. Coussot. Drag on a sphere moving through an aging system. *Europhys. Lett.*, **78**:68007, 2007.
 43. J. Feng, P.Y. Huang, and D.D. Joseph. Dynamical simulation of sedimentation of solid particles in an oldroyd-b fluid. *J. non-Newt. Fl. Mech.*, **63**:63–88, 1996.
 44. S. Daugan, L. Talini, B. Herzhaft, and C. Allain. Aggregation of particles settling in shear-thinning fluids. Part 1. Two-particle aggrega-

- tion. *Euro. Phys. J. E*, **7**:73–81, 2002.
45. B. Gueslin, L. Talini, B. Herzhaft, Y. Peysson, and C. Allain. Aggregation behavior of two spheres falling through an aging fluid. *Phys. Rev. E*, **74**:042501, 2006.
 46. B. Dollet, M. Durth, and F. Graner. Flow of foam past an elliptical obstacle. *Phys. Rev. E*, **73**:061404, 2006.
 47. J. Wang and D.D. Joseph. Potential flow of a second-order fluid over a sphere or an ellipse. *J. Fl. Mech.*, **511**:201–215, 2004.
 48. K. Brakke. 200,000,000 Random Voronoi Polygons. www.susqu.edu/brakke/papers/voronoi.htm, 1986. Unpublished.
 49. N. Kern, D. Weaire, A. Martin, S. Hutzler, and S.J. Cox. Two-dimensional viscous froth model for foam dynamics. *Phys. Rev. E*, **70**:041411, 2004.
 50. L. Arnaud, J. Weiss, M. Gay, and P. Duval. Shallow-ice microstructure at Dome Concordia, Antarctica. *Ann. Glaciol.*, **30**:8–12, 2000.
 51. M. Aubouy, Y. Jiang, J.A. Glazier, and F. Graner. A texture tensor to quantify deformations. *Granular Matter*, **5**:67–70, 2003.
 52. A. Kabla and G. Debregeas. Quasi-static rheology of foams. part 1. oscillating strain. *J. Fluid Mech.*, **587**:23–44, 2007.
 53. O. Hassager. Negative wake behind bubbles in non-Newtonian liquids. *Nature*, **279**:402–403, 1979.